SUSPENSION MECHANISMS OF SOLID PARTICULATES IN A HORIZONTAL TURBULENT CHANNEL FLOW

K. T. Kiger *
Department of Mechanical Engineering
University of Maryland
College Park, MD, 20742 USA
kkiger@eng.umd.edu

C. Pan
Department of Mechanical Engineering
University of Maryland
College Park, MD, 20742 USA
chpan@eng.umd.edu

ABSTRACT

INTRODUCTION

Particle/wall turbulence interaction is an important topic to many natural and industrial processes such as particle deposition in materials processing, pneumatic transport of granular materials, and sediment transport within rivers and marine flows. Although much work has been done on this topic, there are still many aspects of the particle turbulence interaction within the wall bounded region that is only known qualitatively, or under limited conditions due to restrictions by existing technology or theoretical simplifications. One such important area is the particle-fluid interaction mechanism that is responsible for the suspension and sedimentation of relatively large, heavy particulates within horizontal, wall-bounded shear flow. Since the development of the contemporary understanding of turbulent burst and sweep structures within boundary layers, it has been speculated that this mechanism is primarily responsible for the for the suspension and interaction of the particles within the flow (Sumer & Oğuz, 1978; Sumer & Diegaard, 1981; Rashidi, et al, 1990; Niño & Garcia, 1996). While this work has revolutionized our phenomenological understanding of the flow, continued model development has not matched this progress due to a lack of quantitative measures of these processes.

In light the of the above discussion, the current work has focused on trying to resolve some of these issues by utilizing a unique image separation technique (Kiger & Pan, 2000) to make simultaneous PIV measurements of both the particulate and carrier phase. These measurements allow for the quantification of the important particle/fluid interaction statistics, as well as providing representative instantaneous vector fields of the carrier fluid structure responsible for the interaction. This paper will briefly present a few preliminary results concerning the mean fluid and particle properties, discuss the statistical structure of the particle suspension, and present several quantitative flow maps that allow for limited interpretation of the particle/turbulence interaction during the suspension process.

EXPERIMENTS

The experiments were performed in a transparent, horizontal, planar water channel with a height ($2h$), width, and length of $4\times36\times488$ cm, respectively. The centerline velocity was approximately 58 cm/s, and pressure gradient measurements indicated the flow was fully developed over the last half of the channel length. The friction velocity for the single-phase case, $u^+ = (\tau_w/\rho)^{1/2}$, was calculated from the the fully developed pressure gradient (measured with a differential pressure transducer along 15 equally spaced stations), giving a value 2.8 cm/sec, and a Reynolds number, $Re_\tau = u^*h/\nu = 570$. A comparison of the single-phase flow conditions was made to the numerical DNS simulations of Moser, Kim, and Mansour (1999), which are shown in Figure 1. The results for the streamwise mean flow are

*corresponding author

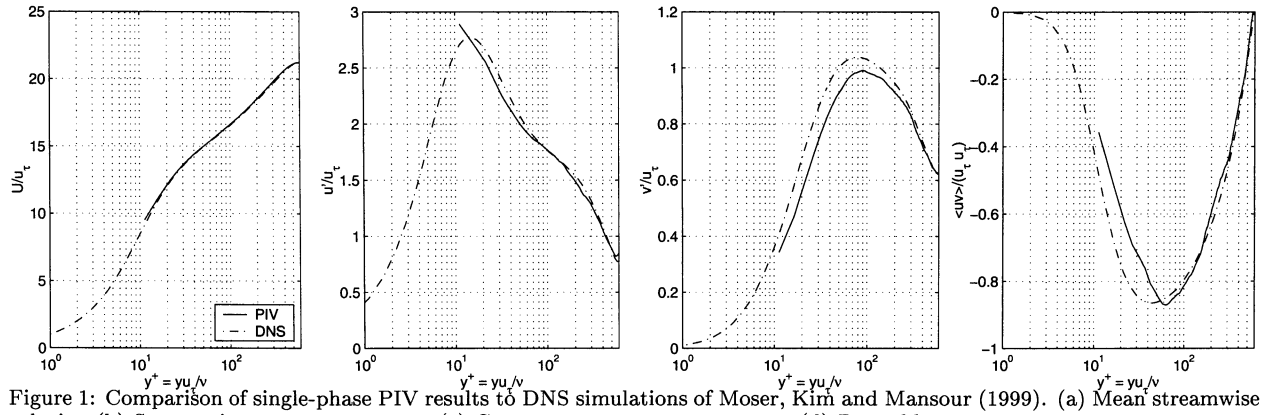

Figure 1: Comparison of single-phase PIV results to DNS simulations of Moser, Kim and Mansour (1999). (a) Mean streamwise velocity, (b) Streamwise r.m.s. component, (c) Cross-stream r.m.s. component, (d) Reynolds stress.

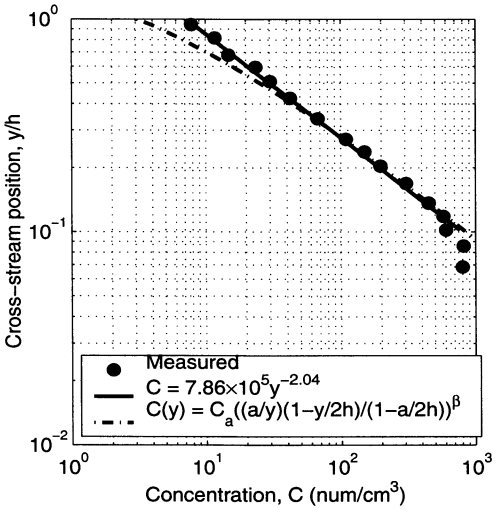

Figure 2: Mean sediment concentration profile.

indistinguishable from the simulation, with less than a 1% deviation over the range of the measurement. The streamwise fluctuating velocity agrees to within 5%, while the cross-stream variation and Reynolds stress is within 5% for $y^+ > 70$, and to within 15% for $20 < y^+ < 70$. The DNS data serves as a useful benchmark for qualifying the design of the channel as well as assessing the quality of the PIV images and processing algorithms used in the analysis.

For the two-phase flow, glass beads with a specific gravity of 2.6 and a nominal diameter of 200 μm were seeded within the contraction inlet section to the channel. The particles were distributed uniformly across the span of the channel prior to entering the water using a series of 8 screens suspended above the settling chamber. The mass flow of the particles was approximately 0.004 kg/s, giving a bulk loading ratio of 5×10^{-4}.

A series of 455 image pairs of the flow field were acquired using a Kodak ES-1.0 camera (1008×1018 pixel imager), once the particle flux appeared to have reached a steady state within the channel. Long streamwise streak structures were clearly visible within the channel, which is in agreement with observations by other researchers (Rashidi, *et al*, 1991; Niño and Garcia, 1996). The images were processed using a median filter to separate the phases (filter width of 5 pixels). Cross-correlation PIV was used to obtain the carrier fluid motion, and discrete particle tracking was performed to extract the particle location and velocity. Approximately 15,000 dispersed phase particles were tracked within the image set, and selective conditionally sampled statistics of the carrier fluid were obtained at the particle locations using a cubic spline interpolation to the nearest fluid vectors.

RESULTS AND DISCUSSION

Mean Concentration

Selected profiles calculated from the data are shown in Figures 2–6. Figure 2 depicts the mean concentration profile, estimated from the number of particles imaged within the light-sheet and field of view of the camera. The profile appears to be well fit with a power law distribution outside of the high concentration region near the wall, and is adequately represented by a distribution given by Rouse (1937)

$$\frac{C}{C_a} = \left(\frac{a}{y}\frac{(1-y/h)}{(1-a/h)}\right)^{\beta}, \qquad (1)$$

where, a is a reference position (taken to be $a/h = 0.1$ in the current example), and $\beta = v_s/\kappa u^+ = 1.9$ using the clear-water value for the Von Karman constant, $\kappa = 0.41$, the friction velocity, an approximate fit to the log layer of the two-phase fluid velocity to obtain the friction velocity, $u^+ = 3.2$ cm/s, and the particle settling velocity, $v_s = 2.5$ cm/s. The curve tends to diverge from the data in the upper portion of the channel, which may be due to a combination of the facts that the original equation was derived for open channel flow.

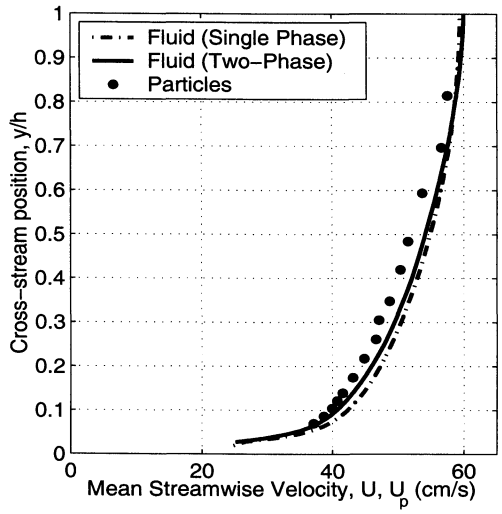

Figure 3: Streamwise mean velocity profiles of the fluid (with particles present), the dispersed phase particles, and the clear (single-phase) fluid.

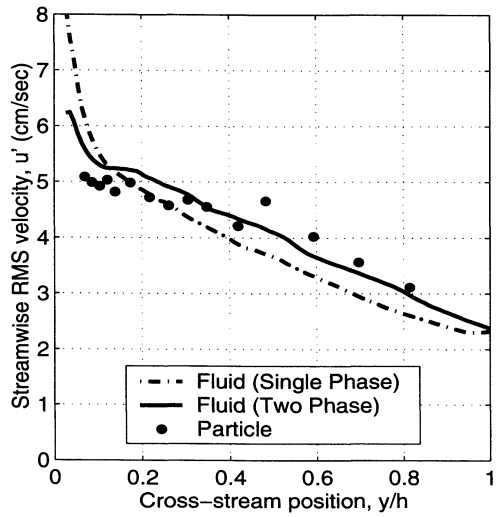

Figure 4: Streamwise turbulent normal stress profiles of the fluid (with particles present), u'_f, the dispersed phase particles, u'_p, and the clear (single-phase) fluid, u'.

Mean Fluid and Particle Velocities

The mean streamwise velocity is plotted for the dispersed and carrier phase as well as the clear water value in Figure 3. As can be seen, the presence of the particles does noticeably alter the mean velocity of the fluid by slightly decreasing the mean velocity over the mid-region of the profile. This results in a concomitant increase in the velocity gradient outside the buffer region, and is consistent with alterations to the flow made by a rough surface (Tachie, *et al*, 2000). It is also noted that the particulate velocity consistenly lags the fluid within the region of measurement. This is similar to the mean particle velocity profiles measured for low density ratio particles ($\rho_p/\rho_f = 1.05$) in a horizontal open channel flow (Kaftori, *et al*,

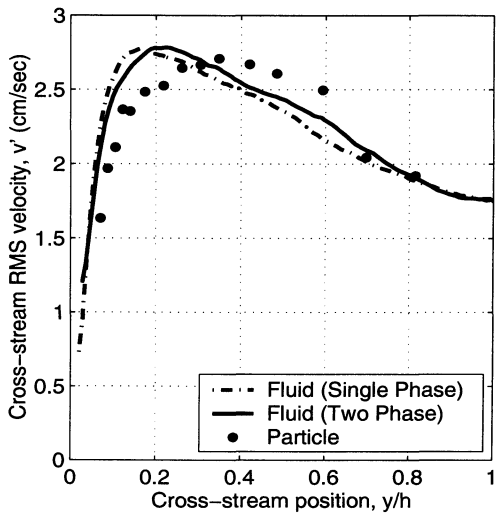

Figure 5: Cross-stream turbulent normal stress profiles of the fluid (with particles present), v'_f, the dispersed phase particles v'_p, and the clear (single-phase) fluid, v'.

1995), as well as the results from large density ratio particles ($\rho_p/rho_f = 8800$) in vertical channels, provided the mass loading is greater than 10% (Kulick, *et at*, 1994). The exception to this is that the large density ration case indicated that the particle velocity was increase with respect to the fluid velocity in the region close to the wall.

Kulick *et al* (1994) made the convincing argument that transverse mixing of large Stokes number particles (where $St = \tau_p/\tau_f$) across a strong gradient will result in a flatter velocity profile for the particles than the fluid owing to their inability to adjust as they are mixed transversly across the channel. In the case of the horizontal channel, however, the relative Stokes numbers were much smaller (approximately 0.01 for Kaftori *et al* (1995), and 0.1 for the current experiments, as compared to 50 for Kulick *el at*, when $\tau_f = h/2U_c$), which would imply that the above arguments would not hold. Instead the similarities in the outer region may result from the asymmetry introduced by having the gravitational forcing normal to the channel wall.

Figure 4, 5, and 6 depict the wall-normal profiles of the streamwise and wall-normal velocity fluctuations and the Reynolds stress for the carrier fluid, the dispersed phase, and the clear water (single-phase) conditions. The trends for the three components are similar, with the particles exhibiting a reduced fluctuation level near the wall in comparison to the fluid, with a slight overshoot of the fluctuation levels in the region $y/h > 0.3$. These results are different from the low density ratio horizontal experiments of Kaftori, *et al* (1995),

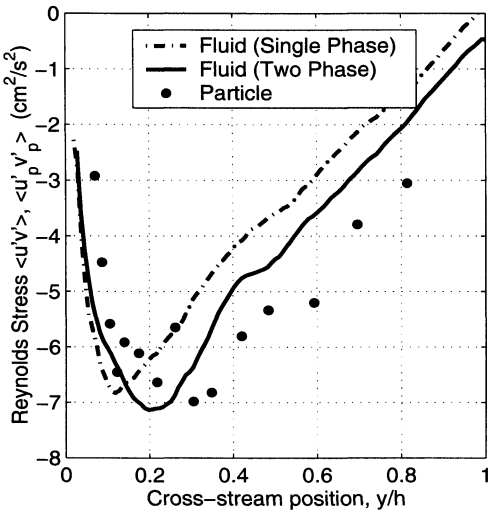

Figure 6: Reynolds Stress profiles of the fluid (with particles present), $u'_f v'_f$, the dispersed phase particles $u'_p v'_p$, and the clear (single-phase) fluid, $u'v'$.

who observed no change in the fluctuation levels except for the wall-normal component close to the boundary, which was increased for their largest particles sizes. Likewise, in the vertical channel experiments of Kulick, *et al* (1994), the streamwise particulate fluctuation levels were the same as the fluid flow at low loadings, but tended to increase at large loading values, while the wall-normal component was everywhere dampened. The current results represent an intermediate Stokes number case between the existing studies, and therefore likely to have a different set of dynamics. The effect of the particles on the fluid is also evident, showing an increase in the fluctuating components at distances greater than $y/h > 0.2$, and a slight damping closer to the wall.

Current effort is being planed on repeating the experiments to increase the statistical convergence of the above preliminary data.

Particle/Fluid Suspension

In order to gain a more direct indication of what, if any, portion of the turbulent busting event is correlated with the suspension of the particles, quadrant plots of the carrier fluid velocity fluctuations sampled at the dispersed phase particle locations is presented in Figure 7. The top set of figures shows the conditional fluid fluctuations within the log region, at $37 < y^+ < 44$. At this location, the majority of the upward moving particles (fluid conditioned on $v_p > 0$) are contained within the second quadrant (Q2), which corresponds to an ejection of slow moving fluid from the wall and is in agreement with mechanisms postulated by previous workers who examined only the motion of the dispersed phase (Sumer and Oğuz, 1978; Sumer and Deigaard, 1981; Niño and Garcia, 1996). A smaller percentage of the particles are located in the first quadrant, and virtually no particles occur within quadrants three and four. This is consistent with the fact that the fluid must typically be moving up to entrain the particles, but also indicates that it is preferentially done in regions of slow moving fluid, likely coming from low-speed streaks. The downward moving particles, on the other hand, are more evenly distributed among the four quadrants at this y^+ location, showing a slight preference for high-speed sweeps of fluid moving toward the wall (Q4). As a result of the net settling velocity of the particles, it is possible to have sediment drifting downwards within upward moving events (note that the upper boundary is approximately at $v_s = 2.5$ cm/s). In addition to this, the similar nature of the distribution to the unconditionally sampled fluid indicates that it is not likely that a single type of event is associated with the return of the particles towards the wall — which would be consistent with a nominal percemtage of the particles drifting back towards the wall after losing correlation with a Q2 uplift event.

At larger y^+ values in the outer flow (Figure 7, bottom figure), there is a more distinct separation of the motions responsible for the particle behavior. The unconditional fluid distribution becomes more circular with the absence of a high shear. The upward moving particles are once again contained in the first two quadrants, but the downward moving ones are now almost exclusively contained within quadrants three and four.

Several of the structures responsible for the suspension process can be observed in Figure 8, which provides individual composite vector fields the fluid velocity, particle location and velocity, superimposed on a contour map of the instantaneous negative Reynolds stress contributions (solid lines) and the kinematic swirl intensity (filled contours). Here the kinematic swirl is a threshold of imaginary eigenvalue component of the deformation rate tensor (Adrian, *et al*, 2000b), and indicates regions of strong circular rotational motion while filtering out regions of dominant shear strain. These figures clearly show several strong Q2 events which are associated with the suspension of sediment particles from the log layer into the outer region of the flow, as implicated by the probability distributions of Figure

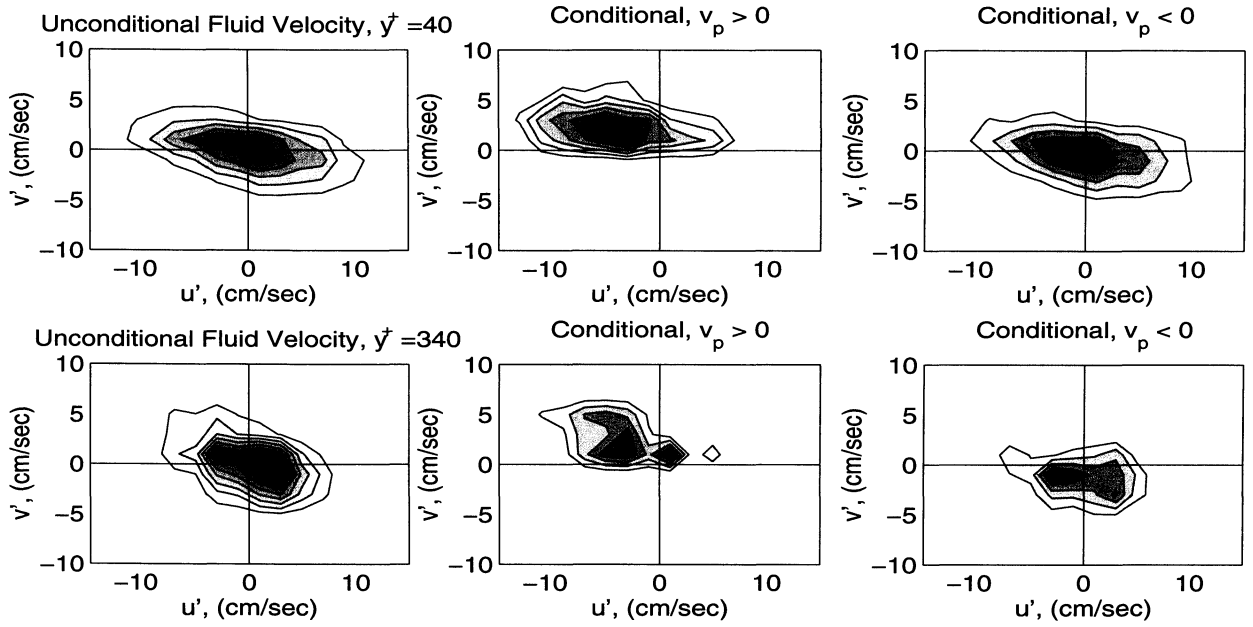

Figure 7: Probability distribution functions of two-phase fluid, fluid velocity conditioned on upward moving particles, and fluid velocity conditioned on downward moving particles. a) $y^+ \approx 40$, and b) $y^+ \approx 340$.

7. The structures observed in the top two maps are reminiscent of isolated hairpin structures and hairpin packets as identified using a similar procedure in a zero-pressure-gradient boundary layer by Adrian, *et al* (2000a). It is interesting to note that while these structures did appear in the current experiment, they did not appear as common as reported for the boundary layer case. Although a rigorous study was not performed, the conditions typified by the top two figures occured in perhaps 30% of the images, as opposed to 85% of the images as reported by Adrian, *et al* (2000).

Other structures that were observed include pairs of spanwise counter-rotating swirls which seemed to form a jet entraining slow-momentum fluid upstream into the oncoming flow (boxed regions in bottom two figures). Although a fair amount of evidence exits to substantiate the hairpin packet mechanism, it is not currently clear as to whether the observed "jets" result from packet interaction, vorticity migrating from the opposing sidewall, the continual generation of vorticity imposed by the mean pressure gradient of the channel, or the modification of the wall sturctures by the sediment. With the limited two-dimensional, single-plane data currently on hand, it is not yet possible to accurately speculate on the source of these additional features. Future work will progress on implementing multi-dimensional measurements to aid in the construction of a more complete mechanistic description.

ACKNOWLEDGEMENTS

The authors would like to thank the National Science Foundation for their generous support of this work under grant number CTS9702723 and instrumentation grant CTS9871156 (program manager M. C. Roco).

References

Adrian, R. J., Meinhart, C. D., & Tomkins, C. D., (2000a) "Vortex organization in the outer region of the turbulent boundary layer," *J. Fluid Mech.*, **422**, pp. 1–54.

Adrian, R. J., Christensen, K. T., & Liu, Z.-C., (2000b) "Analysis and interpretation of instantaneous turbulent velocity fields," *Exp. Fluids*, **29**, pp. 275–290.

Kaftori, D., Hetsroni, G., & Banerjee, S., (1995) "Particle behavior in the turbulent boundary layer. II. Velocity and distribution profiles," *Phys. Fluids*, **7**(5), pp. 1107–1121.

Kiger, K. T. & Pan, C., (2000) "PIV technique for the simultaneous measurement of dilute two-phase flows," *J. Fluids Eng.*, **122**(4), p. 811-818.

Kulick, J. D., Fessler, J. R., & Eaton, J. K., (1994) "Particle response and turbulence modification in fully developed channel flow," *J. Fluid Mech.*, **277**, pp. 109–134.

Moser, R. D., Kim, J., & Mansour, N. N., (1999) "Direct numerical simulation of turbulent channel flow up to Re_τ = 590," *Phys. Fluids*, **11**, pp. 943–945.

Niño, Y., & Garcia, M. H., (1996) "Experiments on particle-turbulence interactions in the near-wall region of an open channel flow: implications for sediment transport," *J. Fluid Mech.*, **326**, pp. 285–319.

Rashidi, M., Hetsroni, G., & Banerjee, S., (1990) "Particle-turbulence interaction in a boundary layer," *Int. J. Multiphase Flow*, **16**(6), pp. 935–949.

Rouse, H., (1937) "Modern conceptions of the mechanics of turbulence," *Trans. Am. Soc. Civ. Eng.*, **102**, p. 436.

Sumer, M., & Oğuz, B., (1978) "Particle motions near the bottom in turbulent flow inan open channel," *J. Fluid Mech.*, **86**, pp. 109-127.

Sumer, M., & Deigaard, R., (1981) "Particle motions near the bottom in turbulent flow in an open channel. Part 2," *J. Fluid Mech.*, **109**, pp. 311–337.

Tachie, M. F., Bergstrom, D. J., & Balachandar, R., (2000) "Rough wall turbulent boundary layers in shallow open channel flow," *J. Fluids Eng.*, **122**, pp. 533–540.

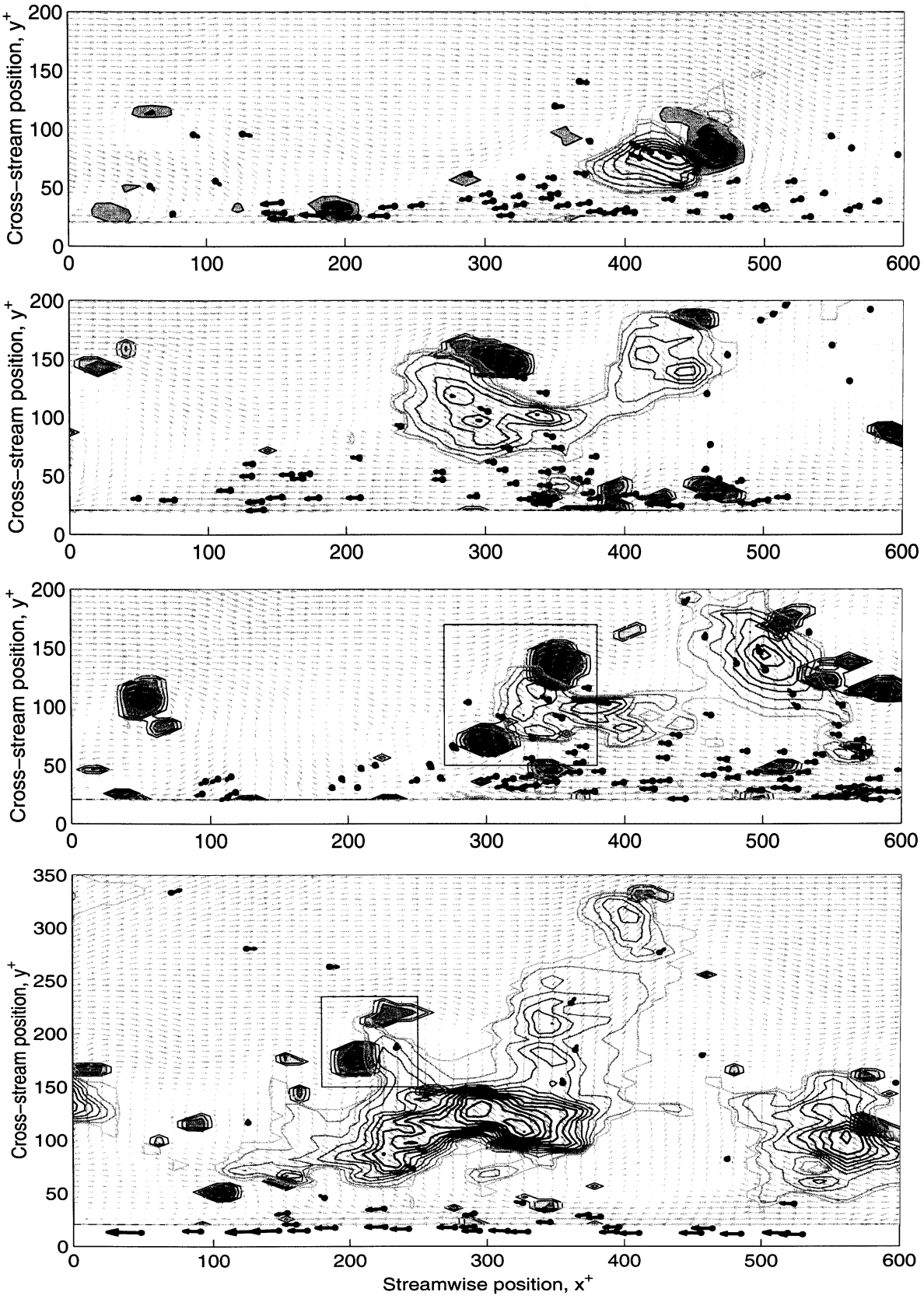

Figure 8: Instantaneous fluid structure map for three realizations of two-phase flow. Fluid vectors are gray, while particle locations and vectors are black. Swirling strength is indicated by the filled gray-level contours, and countours of the Q2/Q4 Reynolds Stress contribution are given by the solid lines.Wall units non-dimensionalization is approximate, and taken from the clear water values.